

Numerical Stability Revisited: A Family of Benchmark Problems for the Analysis of Explicit Stochastic Differential Equation integrators

Thomas Hudson *

Xingjie Helen Li †

Sarah Murphy ‡

March 26, 2025

Abstract

In this paper, we revisit the numerical stability of four well-established explicit stochastic integration schemes through a new generic benchmark stochastic differential equation (SDE) designed to assess asymptotic statistical accuracy and stability properties. This one-parameter benchmark equation is derived from a general one-dimensional first-order SDE using spatio-temporal nondimensionalization and is employed to evaluate the performance of (1) Euler–Maruyama (EM), (2) Milstein (Mil), (3) Stochastic Heun (SH), and (4) a three-stage Runge–Kutta scheme (RK3). Our findings reveal that lower-order schemes can outperform higher-order ones over a range of time step sizes, depending on the benchmark parameters and application context. The theoretical results are validated through a series of numerical experiments, and we discuss their implications for more general applications, including a nonlinear example of particle transport in porous media under various conditions. Our results suggest that the insights obtained from the linear benchmark problem provide reliable guidance for time-stepping strategies when simulating nonlinear SDEs.

Keywords: analysis of explicit numerical integrators for SDEs; asymptotic statistical stability; spatio-temporal nondimensionalization

MSCcodes: 60H35, 65L20

1 Introduction

Stochastic differential equation (SDE) models are important for modelling a wide range of real-world phenomena, and combine both deterministic and random effects into a model describing the evolution of degrees of freedom in time. In many cases, SDE models are ergodic, entailing that the law of the process converges to an equilibrium distribution independently of the initial condition. In practice, ergodicity is a desirable property for real-world applications, with the equilibrium distribution representing a form of thermalised steady-state for a system.

To simulate and predict the behaviour of SDE models, numerical integration algorithms are needed, and a wide range of algorithms have therefore been developed to simulate SDE models. Even when SDE models are ergodic, it has long been established that numerical discretisations of SDEs do not necessarily faithfully reproduce the equilibrium distribution, exhibiting bias in the resulting statistics. For example, when the drift and diffusion coefficients are only locally Lipschitz, explicit approximation methods like Euler-Maruyama can fail to be ergodic, even if the underlying SDE is itself geometrically ergodic [11, 14]. Conversely, when the coefficient vector fields of SDEs are globally Lipschitz, these methods are proven

*Mathematics Institute, University of Warwick, UK (T.Hudson.1@warwick.ac.uk, tinyurl.com/thudso). T. Hudson is grateful for support from the Warwick Mathematics Institute of University of Warwick.

†Department of Mathematics & Statistics, University of North Carolina Charlotte, NC, (xli47@charlotte.edu). X. Li is grateful for partial support by the NSF Award DMS-1847770 and the 2023 UNC Charlotte faculty research grant.

‡Department of Mathematics & Statistics, University of North Carolina Charlotte, NC, (shelfert@charlotte.edu). S. Murphy is grateful for partial support by the NSF Award DMS-1847770.

to strongly and weakly converge [8, 16]. However, due to the prefactors appearing in convergence order estimates, it is not certain whether a higher-order scheme consistently outperforms a lower-order scheme when the time step size is moderately large, i.e. in cases which lie outside the asymptotic regime.

In applications where SDEs are used as a means to generate samples of a particular distribution, Monte Carlo algorithms often use an accept-reject or Metropolis step to counteract the bias inherent in the numerical discretisation [1, 9]. On the other hand, when we are interested not only in sampling the equilibrium distribution but also in the dynamics of the process, performing accept-reject steps on entire trajectory segments may be costly, as they involve discarding expensive-to-compute trajectories of high-dimensional systems of SDEs. An alternative to this approach is instead to ask how accurately and stably numerical schemes are able to capture asymptotic statistical properties of the underlying SDE model. If we are able to quantify the errors committed, and these are at an acceptable level for the required application, we may as a result be able to save computational work. Furthermore, stochasticity and stiffness appear in wide range of physical and chemical systems, and the time-step size is often severely restricted to maintain numerical stability and accuracy when integrating stiff stochastic differential equations with fast diffusion process [4–6].

Classically, the stability of SDE schemes has been measured through an approach known as mean-square stability analysis. This uses homogeneous linear SDEs, i.e. geometric Brownian motion, as a benchmark test, extending the concept of linear stability from deterministic ODEs [8, 17]. In this work, we revisit the underlying assumptions of this stability analysis, and propose a more generic benchmark SDE problem for the study of statistical accuracy and stability properties, namely the one-dimensional equation

$$dx_t = -x_t dt + (1 + \eta x_t) dW_t,$$

where η is a real parameter which controls the relative strength of the multiplicative noise and the stiffness of the deterministic drift. By non-dimensionalising the equation, we show that this benchmark arises generically from a general first-order SDE in one dimension with affine coefficients. As mentioned, this approach contrasts with earlier literature on similar questions [17, 18, 20]; which has tended to use geometric Brownian motion as a benchmark, i.e.

$$dx_t = -x_t dt + \eta x_t dW_t.$$

The study of this latter problem benefits from a simple exact expression for solution trajectories in terms of Brownian motion, but we will argue below that since it represents a less generic situation, it does not necessarily reflect the performance of numerical integration schemes in a realistic nonlinear setting. Despite their superficial similarity, as a stark illustration of the contrast between the two problems, the equilibrium distribution for geometric Brownian motion is always concentrated at $x = 0$ when it exists, while our proposed benchmark includes a wide range of algebraic tail behaviour for the resulting equilibrium distribution.

After deriving the benchmark problem, we use it to analyse the performance of some well-established explicit integration schemes. Our focus on explicit schemes is motivated by the need for integrators which avoid costly implicit steps in high dimensional problems. While there is no simple exact formula for solutions of our test problem, we will see that it is nevertheless simple enough to allow for the explicit computation of both the equilibrium distribution and the evolution of the low-order moments of the law as the process evolves. We choose the latter as metrics for assessing the accuracy of the schemes, reflecting the sorts of statistics which are often of interest to practitioners.

Along with a discussion of the late-time statistical accuracy of the numerical methods considered, we find the range of time-steps for which the methods are stable in the sense that they preserve the boundedness of first and second moments as the number of time steps simulated tends to infinity. This is a feature which we term *statistical stability* to distinguish it from other differing notions [8, 13, 17]. The ranges of time step we find provide us with a meaningful way to compare the stability of methods as the parameter η varies, allowing us to representing a range of relative strengths for the multiplicative noise

and drift. In modeling contexts where long trajectories are important in order to enable the observation of phenomena which would otherwise be out of reach, understanding a predicting the stability of methods are important as a way to allow for increased time-step sizes, which trade accuracy for physical insight which would otherwise not be available.

Finally, to verify the analytical results we obtain, we conclude by performing a range of numerical experiments, and discuss the consequences of our results for a more general application to a nonlinear example of particle transport in porous media.¹

Outline. We now provide a brief guide to the remainder of the paper. In Section 2, we review the numerical schemes we study, and give an overview of established results on their local accuracy properties. In Section 3, we use a nondimensionalisation argument to derive our test problem from a general linear SDE, discussing various exactly computable properties of the resulting equation. In Section 4, we derive expressions for the evolution of discrete statistical moments under various numerical integrations, comparing to the continuous counterparts for the benchmark problem, verifying the results numerically and studying the corresponding stability regions. In Section 5, we demonstrate the utility of our results in the context of a more realistic setting of particle diffusion in porous media, where the drift and diffusion coefficients are both nonlinear.

2 Overview of numerical schemes

We consider the stochastic initial value problem for the scalar autonomous Itô stochastic differential equation (SDE) given by

$$dx_t = f(x_t)dt + g(x_t)dW_t, \quad t \in [0, T]. \quad (2.1)$$

We will assume throughout that the solution is subject to a deterministic initial condition, x_0 .

For the purposes of comparing the numerical schemes we study, we will discretise the simulation time interval into subintervals of fixed length $h = T/N$, and define a discrete time grid $t_n = nh$ for $n = 0, \dots, N$. For the different schemes we discuss, x_n will always be used to refer to the approximation of the solution generated at time t_n . For convenience in describing the numerical schemes below, we also introduce the notation

$$f_n := f(x_n), \quad \text{and} \quad f'_n := f'(x_n),$$

and use analogous expressions g_n, g'_n and g''_n for the relevant functions evaluated at x_n . We also introduce sequences of independent identically distributed Gaussian random variables ΔW_n and $\tilde{\Delta W}_n$ with mean zero and variance h , i.e. $\Delta \tilde{W}_n, \Delta W_n \sim \mathcal{N}(0, h)$.

We select four classical explicit numerical schemes to study with a range of levels of accuracy. In particular, we consider:

1. The Euler–Maruyama (EM) method [10], [8, §9.1]:

$$x_{n+1} = x_n + f_n h + g_n \Delta W_n. \quad (\text{EM})$$

2. The Milstein (Mil) method [8, §10.3]:

$$x_{n+1} = x_n + f_n h + g_n \Delta W_n + \frac{1}{2} g'_n g_n (\Delta W_n^2 - h). \quad (\text{Mil})$$

3. The Stochastic Heun (SH) method [17]:

$$x_{n+1} = x_n + \frac{1}{2} [F_1 + F_2] h + \frac{1}{2} [G_1 + G_2] \Delta W_n, \quad (\text{SH})$$

where setting $F(x) := f(x) - \frac{1}{2} g'(x)g(x)$, the coefficients in the relation above are defined to be

$$\begin{aligned} F_1 &= F(x_n), & G_1 &= g(x_n), \\ F_2 &= F(x_n + F_1 h + G_1 \Delta W_n), & G_2 &= g(x_n + F_1 h + G_1 \Delta W_n). \end{aligned}$$

¹All codes can be found at https://github.com/XingjieHelenLi/NumSDE_Revisit.

Method	Strong order	Weak order
Euler-Maruyama (EM)	0.5	1
Milstein (Mil)	1	1
Stochastic Heun (SH)	1	2
3-stage Runge-Kutta (RK3)	3	3

Table 1: A summary of the strong and weak convergence orders of the methods studied. The first two rows correspond to results proved in [8], while the latter two rows correspond to results proved in [16].

4. The improved 3-stage Runge-Kutta (RK3) method [16, 17]:

$$\begin{aligned}
x_{n+1} = & x_n + \frac{1}{4}(F_1 + 3F_3)h + \frac{1}{4}[G_1 + 3G_3]\Delta W_n \\
& + \frac{1}{2\sqrt{3}}\left(f'_n g_n - g'_n f_n - \frac{1}{2}g''_n g_n^2\right)h\Delta\tilde{W}_n,
\end{aligned} \tag{RK3}$$

where we again denote $F(x) := f(x) - \frac{1}{2}g'(x)g(x)$, and the coefficients are

$$\begin{aligned}
F_1 &= F(x_n), & G_1 &= g(x_n), \\
F_2 &= F(x_n + \frac{1}{3}F_1h + \frac{1}{3}G_1\Delta W_n), & G_2 &= g(x_n + \frac{1}{3}F_1h + \frac{1}{3}G_1\Delta W_n), \\
F_3 &= F(x_n + \frac{2}{3}F_2h + \frac{2}{3}G_2\Delta W_n), & G_3 &= g(x_n + \frac{2}{3}F_2h + \frac{2}{3}G_2\Delta W_n).
\end{aligned}$$

Established results on the strong and weak orders of these schemes are summarised in Table 1, and the accuracy in terms of time-stepping h are summarised in Table 2. As we can see, these schemes range significantly across the convergence order that they exhibit.

3 Derivation of benchmark problem

To analytically compare the methods (EM), (Mil), (SH) and (RK3), we focus on a test problem where f and g are time-independent and affine in the spatial variable, i.e.

$$f(x) = -\alpha - \beta x \quad \text{and} \quad g(x) = \gamma + \delta x.$$

In other words, we consider the SDE

$$dx_t = -(\alpha + \beta x_t)dt + (\gamma + \delta x_t)dW_t, \tag{3.1}$$

which is the most general form of autonomous SDE in one variable with coefficients which are affine in x_t , driven by a single Brownian motion. This problem can be seen as the linearised form of the general nonlinear autonomous SDE (2.1) about some fixed spatial point.

In this section, we perform what amounts to a nondimensionalisation of this equation, which allows us to reduce the equation to a single parameter family in the most general case. We also discuss properties of the resulting reduced equation.

3.1 Reduction of cases

We proceed by rescaling and shifting time and space coordinates from (x, t) to (ξ, τ) . To do so, we define $\xi_\tau := Ax_t + B$, and we introduce the time rescaling $t = T\tau$. Here A, B and T are real parameters to be chosen, and $T > 0$ is positive, so that the direction of time is preserved. Substituting appropriately, and using the properties of Brownian motion, we obtain the following equation in the new coordinates

$$d\xi_\tau = -(TA^{-1}(\alpha + \beta B) + \beta T\xi_\tau)d\tau + T^{1/2}A^{-1}(\gamma + \delta B + \delta A\xi_\tau)dW_\tau.$$

If $\beta \neq 0$, then we can set $B = -\alpha/\beta$ and $T = 1/|\beta|$ and obtain

$$d\xi_\tau = -\frac{\beta}{|\beta|}\xi_\tau d\tau + \left(\frac{\beta\gamma - \alpha\delta}{A\beta|\beta|^{1/2}} + \frac{\delta}{|\beta|^{1/2}}\xi_\tau\right)dW_\tau.$$

Next, as long as $\beta\gamma - \alpha\delta \neq 0$, we can set $A = \frac{\beta\gamma - \alpha\delta}{\beta|\beta|^{1/2}}$ and $\eta := \frac{\delta}{|\beta|^{1/2}}$ to obtain

$$d\xi_\tau = \pm\xi_\tau d\tau + (1 + \eta\xi_\tau)dW_\tau, \quad (3.2)$$

where the sign of the term in front of the drift term is opposite to that of β . Equation (3.2) provides the most generic dimensionless form of (3.1) in this sense, but there are other possible cases:

- If $\beta \neq 0$ but $\beta\gamma - \alpha\delta = 0$, then we can rescale to obtain geometric Brownian motion

$$d\xi_\tau = \pm\xi_\tau d\tau + \eta\xi_\tau dW_\tau, \quad (3.3)$$

where again $\eta = \frac{\delta}{|\beta|^{1/2}}$.

- If $\beta = 0$ but $\delta \neq 0$, then we can set $B = -\gamma/\delta$, $T = |\delta|^{-1/2}$ and $A = -\alpha|\delta|^{1/2}$ to obtain

$$d\xi_\tau = d\tau \pm \xi_\tau dW_\tau. \quad (3.4)$$

- Finally, we could have $\beta = 0$ and $\delta = 0$, resulting in an equation which is simply a translation of a Brownian motion.

In the existing literature on the numerical analysis of SDEs with multiplicative noise, geometric Brownian motion (3.3) has been used as a common test equation for numerical methods. A likely reason for the use of geometric Brownian motion is the availability of an analytical solution; the derivation above shows however that both this case and the case where (3.4) is the resulting equation form sets of zero measure in the four-dimensional space of parameters α , β , γ and δ . As such, we choose to focus on consideration of (3.2) for $\eta \in \mathbb{R}$ throughout the remainder of this work.

3.2 Equilibrium distribution

There are a range of established approaches which can be used to demonstrate that the SDE is ergodic with respect to an equilibrium distribution. One such approach is provided [11], which in turn relies upon the methodology introduced by [3, 12].

The Fokker–Planck equation which governs the probability density function p of solutions to the model problem (3.2) is the PDE

$$\partial_t p = \partial_x \left(xp + \partial_x \left(\frac{1}{2}(1 + \eta x)^2 p \right) \right).$$

In particular, this would require the verification of a *minorisation condition* for the transition kernel of the process, and the construction of a *Lyapunov function*. In the case of this equation $V(x) = \sqrt{1 + x^2}$ acts as a Lyapunov function, and the fact that the minorisation condition can be holds shown to a consequence of Hörmander’s theorem [7], but a detailed verification of the conditions required to prove ergodicity is not within the scope of the present work.

Instead, we focus here on formally computing the equilibrium distribution, which is a steady state of the Fokker–Planck equation. In the case we focus on, the Fokker–Planck equation is

$$\partial_t p = \partial_x \left(xp + \partial_x \left(\frac{1}{2}(1 + \eta x)^2 p \right) \right). \quad (3.5)$$

If the SDE is ergodic, then there is an integrable steady state of this equation, p_∞ , such that no matter what distribution the process has at initial time, $p \rightarrow p_\infty$ as $t \rightarrow +\infty$. To identify the equilibrium distribution, we consider the equation

$$0 = \partial_x \left(xp_\infty + \partial_x \left(\frac{1}{2}(1 + \eta x)^2 p_\infty \right) \right) = \partial_x \left((\eta + (\eta^2 + 1)x) p_\infty + \frac{1}{2}(1 + \eta x)^2 \partial_x p_\infty \right).$$

We note that the coefficient of the highest order terms in this equation vanish when $x = -\frac{1}{\eta}$, and this reflects the compact support of the solution p_∞ when $\eta \neq 0$. Integrating once and rearranging, we have

$$\frac{A}{(1 + \eta x)^2} = \frac{2\eta + 2(\eta^2 + 1)x}{(1 + \eta x)^2} p_\infty + \partial_x p_\infty,$$

where A is some constant. Multiplying through by the integrating factor

$$I(x) := \exp\left(\int^x \frac{2\eta + 2(\eta^2 + 1)u}{(1 + \eta u)^2} du\right) = \exp\left(\frac{2}{\eta^2} \frac{1}{1 + \eta x}\right) (1 + \eta x)^{2 + \frac{2}{\eta^2}},$$

we have that

$$A \exp\left(\frac{2}{\eta^2} \frac{1}{1 + \eta x}\right) (1 + \eta x)^{\frac{1}{\eta^2}} = \partial_x (I(x)p_\infty(x)).$$

We note that the term on the right hand side is not integrable in a neighbourhood of $x = -\frac{1}{\eta}$, so we must have that $A = 0$. Integrating again it follows that

$$p_\infty(x) = \frac{B}{I(x)} = B \exp\left(-\frac{2}{\eta^2} \frac{1}{1 + \eta x}\right) (1 + \eta x)^{-2 - \frac{2}{\eta^2}},$$

for some coefficient B , and to normalise appropriately, we can integrate. For now, assuming that $\eta > 0$ and making the change of variable $y = \frac{2}{\eta^2} \frac{1}{1 + \eta x}$, we can express the integral using the Gamma function as

$$\int_{-\frac{1}{\eta}}^{\infty} \exp\left(-\frac{2}{\eta^2} \frac{1}{1 + \eta x}\right) (1 + \eta x)^{-2 - \frac{2}{\eta^2}} dx = 2^{-\frac{2}{\eta^2}} \eta^{-1 + \frac{4}{\eta^2}} \Gamma\left(\frac{2}{\eta^2}\right).$$

The density of the properly normalised form of the equilibrium distribution is therefore

$$p_\infty(x) = \begin{cases} \frac{2^{\frac{2}{\eta^2}} \eta^{1 - \frac{4}{\eta^2}}}{\Gamma\left(\frac{2}{\eta^2}\right)} \exp\left(-\frac{2}{\eta^2} \frac{1}{1 + \eta x}\right) (1 + \eta x)^{-2 - \frac{2}{\eta^2}} & x > -\frac{1}{\eta} \\ 0 & x \leq -\frac{1}{\eta} \end{cases} \quad (3.6)$$

If $\eta < 0$, then we obtain the same form of the equilibrium distribution, but x and η are replaced by $-x$ and $-\eta$ in the definition above. In the special case where $\eta = 0$, the SDE (3.2) has an additive noise term, and the distribution becomes a standard Gaussian with zero mean and variance $\frac{1}{2}$.

Remark 3.1 *Due to the algebraic decay of the tail of this distribution as $x \rightarrow +\infty$, we note that the k th moment of the equilibrium distribution is only well-defined when $x^k p_\infty(x)$ is integrable, which requires*

$$k - 2 - \frac{2}{\eta^2} < -1, \quad \text{i.e.} \quad |\eta| < \sqrt{\frac{2}{k-1}}.$$

We can also explicitly calculate that the first and second moments of the equilibrium distribution are

$$\mu_\infty^{(1)} = \int_{-\infty}^{\infty} x p_\infty dx = 0 \quad \text{and} \quad \mu_\infty^{(2)} = \int_{-\infty}^{\infty} x^2 p_\infty dx = \frac{1}{2 - \eta^2}; \quad (3.7)$$

the latter moment is only finite for $|\eta| < \sqrt{2}$. We note that, when the second moment is finite, we can infer the value of η up to its sign, and hence identify the equation governing the dynamics within the class of reduced equations (3.2).

3.3 Evolution of moments

In addition to finding the equilibrium distribution, we are also able to use the Fokker–Planck equation (3.5) to find closed form expressions for the evolution of the moments of the distribution of independent solutions to (3.2) over time. In particular, consider the evolution of the first and second moments of the position distribution, defining

$$\mu^{(1)}(t) := \int_{-\infty}^{\infty} xp \, dx \quad \text{and} \quad \mu^{(2)}(t) := \int_{-\infty}^{\infty} x^2 p \, dx.$$

We can now use the Fokker–Planck equation (3.5) to derive equations for these moments. For example, we have

$$\frac{d\mu^{(1)}}{dt} = \int_{-\infty}^{\infty} x \partial_t p \, dx = \int_{-\infty}^{\infty} x \partial_x \left(xp + \partial_x \left(\frac{1}{2}(1 + \eta x)^2 p \right) \right) dx.$$

Formally integrating by parts, we find that the first moment satisfies the ODE

$$\frac{d\mu^{(1)}}{dt} = - \int_{-\infty}^{\infty} xp \, dx - \int_{-\infty}^{\infty} \partial_x \left(\frac{1}{2}(1 + \eta x)^2 p \right) dx = -\mu^{(1)},$$

and a similar argument allows us to show that the second moment satisfies

$$\frac{d\mu^{(2)}}{dt} = -(2 - \eta^2)\mu^{(2)} + 2\eta\mu^{(1)} + 1.$$

If the initial condition is deterministic, so that $p(x, 0) = \delta_{x_0}(x)$, the corresponding initial conditions for these moment equations are $\mu^{(1)}(0) = x_0$ and $\mu^{(2)}(0) = x_0^2$. Solving the first equation, we find that

$$\mu^{(1)}(t) = x_0 e^{-t}.$$

As expected, $\mu^{(1)}(t) \rightarrow 0$ as $t \rightarrow \infty$, and the first moment tends to the first moment of the equilibrium distribution, as expected from the discussion of ergodicity given above.

For the second moment, we can substitute the expression for the first moment and solve, yielding the solutions

$$\mu^{(2)}(t) = \begin{cases} x_0^2 e^{-(2-\eta^2)t} + \frac{1}{2-\eta^2}(1 - e^{-(2-\eta^2)t}) + \frac{2\eta x_0}{1-\eta^2}(e^{-t} - e^{-(2-\eta^2)t}), & \eta \neq \pm 1, \\ x_0^2 e^{-t} + 1 - e^{-t} \pm 2x_0 t e^{-t} & \eta = \pm 1. \end{cases}$$

We observe that the long-time limit of $\mu^{(2)}$ exists only in the case when $\eta^2 < 2$, which corresponds to the case where the second moment of the equilibrium distribution is finite, and in this case $\mu^{(2)}(t) \rightarrow \frac{1}{2-\eta^2}$ as $t \rightarrow \infty$, which is exactly the value given in (3.7).

Remark 3.2 *Even in the case where $\mu^{(2)}$ blows up as $t \rightarrow \infty$, we observe that we can still determine the value of η (up to sign) by observing the exponential growth rate:*

$$\lim_{t \rightarrow \infty} \frac{\log \mu^{(2)}(t)}{t} = \eta^2 - 2.$$

This demonstrates that first and second moment information are sufficient to recover the η parameter which fixes the particular reduced problem (3.2).

4 Statistical stability properties of numerical schemes

We now turn our focus to the asymptotic stability properties of the numerical schemes we consider. To study the asymptotic properties of the numerical schemes considered across a range of time-step sizes h , we define the j th moment at step n to be

$$\mu_n^{(j)} := \mathbb{E}[(x_n)^j].$$

We will focus on the cases where $j = 1$ and $j = 2$, since as we have argued above, these are the moments which together characterise the reduced SDE (3.2). By considering each of the schemes in turn, we will show that we can derive recurrence relations for these moments.

4.1 Asymptotic moment stability

We define the following notion of asymptotic accuracy and stability.

Definition 4.1 For a given time step h , a numerical discretisation scheme of an SDE is said to be asymptotically stable for the j th moment if

$$\limsup_{n \rightarrow \infty} \left| \mu_n^{(j)} - \mathbb{E}[(X_{t_n})^j] \right| < +\infty.$$

A numerical discretisation is said to be asymptotically $O(h^n)$ accurate for the j th moment if for all h sufficiently small,

$$\limsup_{n \rightarrow \infty} \left| \mu_n^{(j)} - \mathbb{E}[(X_{t_n})^j] \right| = O(h^n).$$

Clearly, the latter notion of asymptotic accuracy for the j th moment necessarily requires that there exist some possible values of the time step h for which the scheme is also asymptotically stable for the same moment.

4.2 Euler-Maruyama (EM)

Taking expectations and using the scheme definition (EM) in this case, we find that

$$\mu_{n+1}^{(1)} = \mathbb{E}[x_{n+1}] = \mathbb{E} \left[(1-h)x_n + (1-\eta x_n)h^{1/2} \Delta W_n \right] = (1-h)\mu_n^{(1)},$$

where we have used the fact that x_n and ΔW_n are independent, and hence we can solve to obtain $\mu_n^{(1)} = (1-h)^n x_0$. For the expectation to vanish in the long-time limit, we therefore require that

$$|1-h| < 1, \quad \text{i.e.} \quad 0 < h < 2.$$

As we should expect, this is the classical stability region for the explicit Euler method. When the scheme is asymptotically first moment stable, we have that $\mu_n^{(1)} \rightarrow 0$ as $n \rightarrow \infty$, so there is no asymptotic bias in the scheme.

Following a similar approach for the second moment using independence and the properties of a standard normal random variable to deduce that the cross terms vanish, we have

$$\begin{aligned} \mu_{n+1}^{(2)} &= \mathbb{E}[(x_{n+1})^2] = \mathbb{E}[(1-h)^2 x_n^2] + \mathbb{E}[(1-\eta x_n)^2 (\Delta W_n)^2] \\ &= (1-h)^2 \mu_n^{(2)} + h(1-2\eta \mu_n^{(1)} + \eta^2 \mu_n^{(2)}) \\ &= ((1-h)^2 + h\eta^2) \mu_n^{(2)} + 2h\eta \mu_n^{(1)} + h. \end{aligned}$$

Employing the standard linear stability analysis for discrete dynamical systems, the fixed point is stable when

$$\left| \frac{\partial}{\partial \mu_n^{(2)}} \left[((1-h)^2 + h\eta^2) \mu_n^{(2)} + 2h\eta \mu_n^{(1)} + h \right] \right| = |(1-h)^2 + h\eta^2| < 1;$$

this reduces to the requirement that

$$0 < h < 2 - \eta^2. \tag{4.1}$$

Note that this is (as expected) strictly more restrictive than the requirement that $0 < h < 2$ when only considering the asymptotic stability of the first moment.

If the scheme is asymptotically first and second moment stable under the conditions obtained above, then $\mu_n^{(2)} \rightarrow \mu_\infty^{(2)}$ which solves

$$\mu_\infty^{(2)} = ((1-h)^2 + h\eta^2) \mu_\infty^{(2)} + h \quad \text{and hence} \quad \mu_\infty^{(2)} = \frac{1}{2 - \eta^2 - h} = \mathbb{E}[X_{t_n}^2] + O(h).$$

The asymptotic second moment is therefore asymptotically first-order accurate for the second moment.

4.3 Milstein (Mil)

For the Milstein scheme applied to test equation (3.2), the relevant coefficients are

$$f_n = -x_n, \quad g_n = 1 + \eta x_n \quad \text{and} \quad \frac{1}{2}[g'g]_n = \frac{1}{2}\eta(1 + \eta x_n),$$

so

$$x_{n+1} = (1 - h)x_n + (1 + \eta x_n)\Delta W_n + \frac{1}{2}\eta(1 + \eta x_n)(\Delta W_n^2 - h).$$

Taking expectations, the latter terms on the right-hand side vanish, and as with the Euler-Maruyama scheme, we have

$$\mu_{n+1}^{(1)} = (1 - h)\mu_n^{(1)}.$$

The same step-size restriction therefore applies for asymptotic stability of the first moment, i.e. we require $0 < h < 2$. Similarly, when asymptotically first moment stable, there is no error in the scheme; the limit point is $\mu_\infty^{(1)} = 0$.

To analyse the second moment, we find that after squaring, the expectations of the cross terms again vanish, and we obtain

$$\begin{aligned} \mu_{n+1}^{(2)} &= (1 - h)^2 \mathbb{E}[x_n^2] + \mathbb{E}[(1 + \eta x_n)^2] \mathbb{E}[\Delta W_n^2] + \frac{1}{4}\eta^2 \mathbb{E}[(1 + \eta x_n)^2] \mathbb{E}[(\Delta W_n^2 - h)^2] \\ &= (1 - h)^2 \mu_n^{(2)} + h(1 + 2\eta\mu_n^{(1)} + \eta^2 \mu_n^{(2)}) + \frac{1}{2}h^2\eta^2(1 + 2\eta\mu_n^{(1)} + \eta^2 \mu_n^{(2)}). \end{aligned}$$

Once more, assuming that $\mu_n^{(1)} \rightarrow 0$, the system has a stable fixed point under the condition that

$$\begin{aligned} \left| \frac{\partial}{\partial \mu_n^{(2)}} \left((1 - h)^2 \mu_n^{(2)} + h(1 + 2\eta\mu_n^{(1)} + \eta^2 \mu_n^{(2)}) + \frac{1}{2}h^2\eta^2(1 + 2\eta\mu_n^{(1)} + \eta^2 \mu_n^{(2)}) \right) \right| \\ = |(1 - h)^2 + h\eta^2 + \frac{1}{2}h^2\eta^4| = |1 - (2 - \eta^2)h + (1 + \frac{1}{2}\eta^4)h^2| < 1. \end{aligned}$$

For $h > 0$, this condition can be further reduced to

$$0 < h < \frac{2 - \eta^2}{1 + \frac{1}{2}\eta^4}. \quad (4.2)$$

Note that the latter condition for the stability of the second moment is more restrictive than for EM; compare (4.1). When the scheme is asymptotically second moment stable, the fixed point $\mu_\infty^{(2)}$ must solve

$$\mu_\infty^{(2)} = ((1 - h)^2 + h\eta^2 + \frac{1}{2}h^2\eta^4) \mu_\infty^{(2)} + h + \frac{1}{2}h^2\eta^2,$$

which has solution

$$\mu_\infty^{(2)} = \frac{1 + \frac{1}{2}h\eta^2}{2 - \eta^2 - h(1 + \frac{1}{2}\eta^4)} = \frac{1}{2 - \eta^2} + O(h),$$

and hence the scheme is asymptotically first-order accurate for the second moment.

4.4 Stochastic Heun (SH)

To analyse the SH method, we note that the auxiliary function $F := f - \frac{1}{2}g'g$ is

$$F(x) = -x - \frac{1}{2}\eta(1 + \eta x).$$

Working through the algebra, and taking expectations, we find that

$$\mu_{n+1}^{(1)} = (1 - h + \frac{1}{8}h^2(2 + \eta^2)^2) \mu_n^{(1)} + \frac{1}{8}\eta h^2(2 + \eta^2).$$

In this case, the criterion for first moment stability is

$$|1 - h + \frac{1}{8}h^2(2 + \eta^2)^2| < 1, \quad \text{or} \quad 0 < h < \frac{8}{(2 + \eta^2)^2}.$$

When stable, the limiting fixed point $\mu_\infty^{(1)}$ is

$$\mu_\infty^{(1)} = \frac{\frac{1}{8}\eta h(2 + \eta^2)}{1 - \frac{1}{8}h(2 + \eta^2)^2} = O(h).$$

As such, the SH scheme is asymptotically biased, i.e. it has a first-order accurate asymptotic first moment.

For the second moment, working through the algebra, we obtain the recurrence relation:

$$\begin{aligned} \mu_{n+1}^{(2)} = & \left(h - \frac{1}{2}h^2(2 + \eta^2) + \frac{1}{4}h^3(1 + \eta^2)^2 + \frac{1}{64}h^3\eta^2(2 + \eta^2)^2 \right) \\ & + \left(2h\eta - \frac{1}{4}h^2\eta(10 + 3\eta^2) + \frac{1}{4}h^3\eta(2 + 5\eta^2 + 2\eta^4) + \frac{1}{32}h^4\eta(2 + \eta^2)^3 \right) \mu_n^{(1)} \\ & + \left(1 - h(2 - \eta^2) - \frac{1}{4}h^2((2 + \eta^2)^2 - 12) \right. \\ & \left. + \frac{1}{4}h^3(\eta^6 + 3\eta^4 - 4) + \frac{1}{64}h^4(2 + \eta^2)^4 \right) \mu_n^{(2)}. \end{aligned}$$

This recurrence relation is stable if the first moment converges, and if in addition

$$\left| 1 - h(2 - \eta^2) - \frac{1}{4}h^2((2 + \eta^2)^2 - 12) + \frac{1}{4}h^3(\eta^6 + 3\eta^4 - 4) + \frac{1}{64}h^4(2 + \eta^2)^4 \right| < 1.$$

In this case, the stability region does not have simple closed form expression, and indeed we find that the SH method is in fact stable beyond the region in which the SDE has an asymptotically stable second moment; see Section 4.7 below for further discussion.

Using the asymptotic first moment obtained above and solving to find the fixed point, we obtain that the second moment is first-order accurate, i.e. that

$$\mu_\infty^{(2)} = \frac{1}{2 - \eta^2} + O(h).$$

4.5 3-stage Runge-Kutta

Here, after working through the algebra and taking expectations, we find that

$$\mu_{n+1}^{(1)} = -\frac{1}{24}h^2\eta(2 + 3\eta^2) - \frac{1}{48}h^3\eta(2 + \eta^2)^2 + \left(1 - h + \frac{1}{8}h^2(4 - \eta^4) - \frac{1}{48}h^3(2 + \eta^2)^3 \right) \mu_n^{(1)}$$

The first moment is asymptotically stable whenever

$$\left| 1 - h + \frac{1}{8}h^2(4 - \eta^4) - \frac{1}{48}h^3(2 + \eta^2)^3 \right| < 1,$$

and the fixed point is

$$\mu_\infty^{(1)} = -\frac{h\eta(4 + 6\eta^2 + h(2 + \eta^2)^2)}{48 - 6h(4 - \eta^4) + h^2(2 + \eta^2)^3} = O(h).$$

We therefore see that, like the Heun method, the Runge-Kutta scheme is asymptotically biased, but is asymptotically first-order accurate.

Method	1st moment	2nd moment
Euler-Maruyama (EM)	Exact	$O(h)$
Milstein (Mil)	Exact	$O(h)$
Stochastic Heun (SH)	$O(h)$	$O(h)$
3-stage Runge-Kutta (RK3)	$O(h)$	$O(h)$

Table 2: A summary of the accuracy of the asymptotic moments of the methods studied [8].

For the second moment, we have

$$\begin{aligned}
\mu_{n+1}^{(2)} = & \left(h - \frac{1}{2}h^2(2 - \eta^2) + \frac{1}{12}h^3(8 - \eta^4) - \frac{1}{192}h^4(32 + 20\eta^2 - 44\eta^4 - 27\eta^6) \right. \\
& + \frac{1}{288}h^5(2 + \eta^2)^2(2 + 7\eta^2 + 6\eta^4) + \frac{1}{2304}h^6\eta^2(2 + \eta^2)^4 \\
& + \left(2h\eta - \frac{1}{12}h^2\eta(38 - 9\eta^2) + \frac{1}{24}h^3\eta(56 + 2\eta^2 - 5\eta^4) \right. \\
& \quad \left. - \frac{1}{96}h^4\eta(72 + 44\eta^2 - 50\eta^4 - 27\eta^6) \right. \\
& \quad \left. + \frac{1}{72}h^5\eta(2 + \eta^2)^3(1 + 3\eta^2) + \frac{1}{1152}h^6\eta(2 + \eta^2)^5 \right) \mu_n^{(1)} \\
& + \left(1 - h(2 - \eta^2) + \frac{1}{4}h^2(8 - 8\eta^2 + \eta^4) - \frac{1}{24}h^3(32 - 36\eta^2 + 3\eta^6) \right. \\
& \quad + \frac{1}{192}h^4(2 + \eta^2)^2(28 - 52\eta^2 + 27\eta^4) - \frac{1}{96}h^5(2 + \eta^2)^4(1 - 2\eta^2) \\
& \quad \left. + \frac{1}{2304}h^6(2 + \eta^2)^6 \right) \mu_n^{(2)}.
\end{aligned}$$

The stability criterion in this case is

$$\begin{aligned}
& \left| 1 - h(2 - \eta^2) + \frac{1}{4}h^2(8 - 8\eta^2 + \eta^4) - \frac{1}{24}h^3(32 - 36\eta^2 + 3\eta^6) \right. \\
& \quad \left. + \frac{1}{192}h^4(2 + \eta^2)^2(28 - 52\eta^2 + 27\eta^4) - \frac{1}{96}h^5(2 + \eta^2)^4(1 - 2\eta^2) + \frac{1}{2304}h^6(2 + \eta^2)^6 \right| < 1.
\end{aligned}$$

Again, there is no simple closed form for the solution in this case.

Under the assumption that the first moment is stable, it can be checked that the fixed point for this recurrence relation is

$$\mu_\infty^{(2)} = \frac{1}{2 - \eta^2} + O(h);$$

the full expression is omitted due to its length, but we see that this method is asymptotically first-order accurate for the second moment.

4.6 Summary of results

The statistical accuracy results we have obtained above are summarised in Table 2. We see that despite their higher-order accuracy on trajectories over a fixed time period, the SH and RK3 methods are less accurate in recovering asymptotic moment properties, since they exhibit asymptotic bias.

Meanwhile, from [8, 15, 16], we know the strong and weak order of accuracy of various schemes, which we recall were summarised in Table 1. Note that due to the pre-factor C included in the convergence estimates, a higher order scheme does not guarantee a better approximation regarding the accuracy of asymptotic moments in the long-time simulation.

4.7 Numerical verification

To verify our analytical results, we performed a range of numerical tests. In Figure 1, we compare the analytic first moments to the discrete first moments up to $T = 20$. The plots confirm our calculations that the EM and Mil schemes are asymptotically first moment stable and accurate, as their trajectories

are sufficiently close to the analytic values uniformly as T increases, even when the step size is large at $h = 0.1$, for various η . We also see confirmation that the RK3 and SH schemes are asymptotically biased, with the discrete moments diverging from the analytic moments at a certain time step depending on η and h . We chose to run this test for differing values of $\eta = 0.1, 1.4$, to highlight how the choice of η can affect asymptotic stability. RK3 and SH are more biased for larger η . When $\eta = 1.4$, we see that the asymptotically biased schemes, RK3 and SH, diverge from the true first moment at an earlier time step.

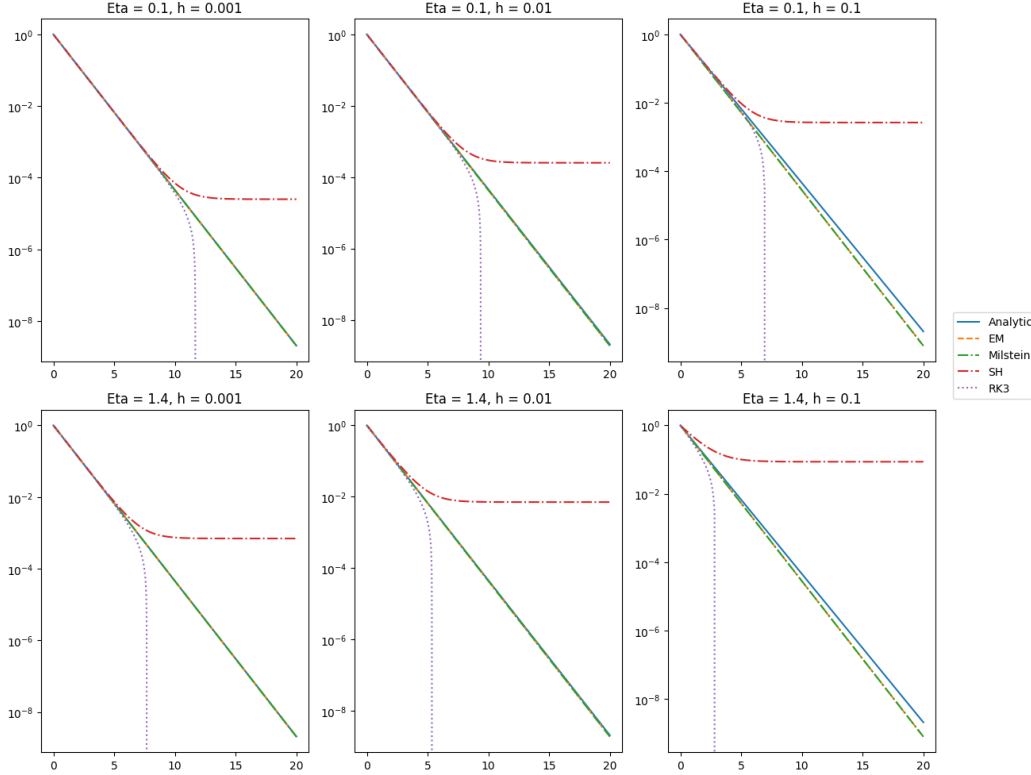


Figure 1: Comparing 1st Moment evolutions up to time $T = 20$ among the analytic and numerical schemes. The first row depicts when $\eta = 0.1$ (Eta) for stepsizes $h = 0.001, 0.01, 0.1$, and the second row depicts when $\eta = 1.4$ with the same range of stepsizes. The moment calculations on the y -axis are plotted on a logarithmic scale. We see that the EM and Milstein schemes are asymptotically first moment stable and accurate, whereas RK3 and SH are biased.

Similarly, in Figure 2, we compare the analytic and discrete second moments up to $T = 20$. Here, with a sufficiently small step size, all schemes show convergence to the true second moment. When h is too large, we see divergence, which is in line with the calculations in this section. Further, when $\eta = 1.4$, the schemes are all more sensitive to the step size, only converging when $h = 0.001$. Also, we see that Milstein is the most asymptotically biased regarding the discrete second moment, and SH is more accurate than RK3 for larger $\eta = 1.4$.

We also conducted a numerical verification of the analytic stability results presented in Section 4, with the results being summarized in Figure 3. For the stability of computing the 1st moment, EM and Mil are the same, and both of them are better than SH; whereas RK3 is more stable than EM and Mil for $\eta \leq 0.5245$, and less stable if $\eta > 0.5245$. For the 2nd moment, EM is always more stable than Mil; and RK3 is always more stable than SH. When η is very small or very large, that is $\eta \leq 0.5$ or $\eta \geq 1.145$, RK3 is more stable than EM, however, for $0.5 < \eta < 1.145$, EM is better.

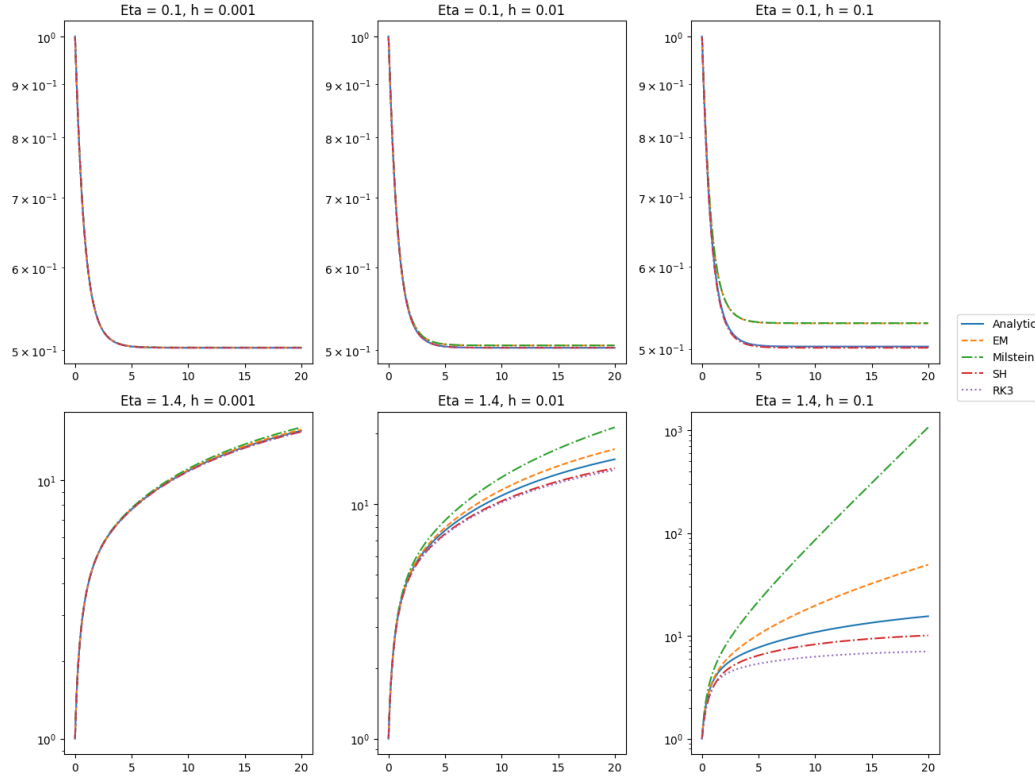


Figure 2: Comparing 2nd Moment evolutions up to time $T = 20$ between analytic and numerical schemes. The first row depicts when $\eta = 0.1$ (Eta) for stepsizes $h = 0.001, 0.01, 0.1$, and the second row depicts when $\eta = 1.4$ with the same range of stepsizes. These plots show that all schemes are asymptotically stable in the second moment, with Milstein being the most biased.

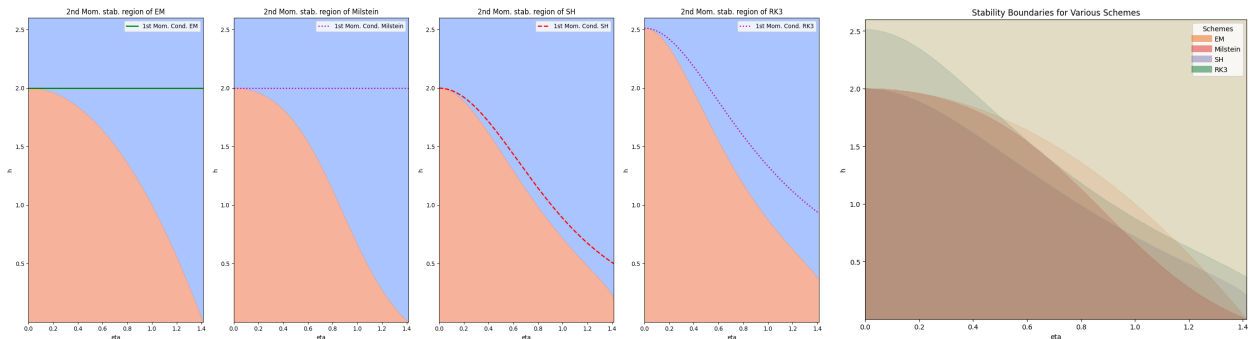


Figure 3: **Subfigs 1–4**: 2nd moment stability regions (pink filled) and 1st moment stability regions (lines below) for EM, Milstein, SH and RK3 schemes. **Subfig 5**: comparison of 2nd moment stability regions among all schemes. Regarding the 1st moment: EM and Milstein are more stable. Regarding the 2nd moment: RK3 is more stable when $\eta \leq 0.5$ or $\eta > 1.145$; and EM is more stable when $0.5 < \eta < 1.145$.

5 Numerical comparison in a nonlinear case

As an illustration of the utility of the benchmark above, we provide a numerical example in this section which is based on a model of particle transport and diffusion in a porous medium.

In a porous medium experiencing steady flow of an incompressible fluid where the velocity in a domain is $\mathbf{u}(\mathbf{x})$, conservation of mass entails that

$$\nabla \cdot \mathbf{u} = 0.$$

Under the assumption that the flow can be modeled by the Darcy relation, we assume that there exists a scalar permeability (or hydraulic conductivity) field $k(\mathbf{x})$ such that \mathbf{u} is locally proportional to the pressure gradient, i.e.

$$\mathbf{u} = -\frac{k}{\mu} \nabla p,$$

where p is the fluid pressure field and μ is the kinematic viscosity of the fluid. Substituting this relation into the equation above, and including the possibility of mass removal by adding a sink term Q to the right-hand side, we find that the pressure must satisfy

$$\nabla \cdot (k \nabla p) = Q.$$

To close the problem to find p (and hence \mathbf{u}), fixed Dirichlet boundary conditions specifying the pressure or Neumann conditions prescribing the flux and thereby the velocity at the boundary can be applied.

To model the transport non-interacting particles which are passive in the flow, it is common to assume that they are advected by the flow field and simultaneously experience molecular diffusion. As such, the motion of such a particle can be represented by the SDE system

$$d\mathbf{X}_t = \mathbf{u}(\mathbf{X}_t)dt + \sigma(\mathbf{X}_t)d\mathbf{W}_t, \quad (5.1)$$

where \mathbf{u} is the velocity field found above, and $D = \frac{1}{2}\sigma^2$ is a scalar molecular diffusion coefficient.

In practice, empirical laws are used to determine the diffusivity and permeability in a medium, often interpolating between empirical measurements made at test boreholes in the field. Here in 1D, we choose to use two particular relations to express diffusivity and permeability in terms of porosity φ , which is the volume fraction of the porous medium which is void. To obtain a particular form, we make the constitutive assumptions that molecular diffusivity in the porous medium follows Bruggeman's relation for a medium made up of spherical obstacles [19], and the permeability follows the Kozeny-Carman equation [2], which results in the following

$$\sigma = \sqrt{2D_0\varphi^{3/2}} \quad \text{and} \quad k = \frac{\varphi^3}{S^2(1-\varphi)^2}, \quad (5.2)$$

where D_0 is the free diffusivity and S is an effective area parameter, we obtain that

$$\nabla \cdot \left(\frac{\varphi^3}{S^2(1-\varphi)^2} \nabla p \right) = Q, \quad \mathbf{u} = -\frac{\varphi^3}{S^2(1-\varphi)^2} \nabla p \quad \text{and} \quad \sigma = \sqrt{2D_0\varphi^{3/2}}. \quad (5.3)$$

Then, assuming we know φ , S and D_0 along with the flow conditions at the boundary of an appropriate domain, we can find the velocity field \mathbf{u} and the diffusion coefficient throughout the domain, and use these fields to simulate particle motion over time.

5.1 A one-dimensional test case

For concreteness, we consider flow in a thin channel aligned with the x -axis containing a porous medium with variable porosity $\varphi(x)$. For simplicity, we consider only the axial flow, and in this case the pressure solves the ODE problem

$$\begin{aligned} \frac{d}{dx} \left(\frac{\varphi^3}{\mu S^2(1-\varphi)^2} \frac{dp}{dx} \right) &= Q(x), \quad 0 < x < L, \\ p(x) &= 0, \quad x = 0, L. \end{aligned} \quad (5.4)$$

Moreover, $u(x) = \frac{-\varphi^3}{S^2(1-\varphi)^2} \frac{dp}{dx}$. If Q is a sink, then it is natural to expect that the pressure reaches a minimum close to the point at which the minimum value of $Q(x)$ is achieved. At such a minimum point, $\frac{dp}{dx}$ vanishes, so the velocity is zero and so particles will tend to flow to this location and accumulate there.

Choosing parameters φ, S, D_0 and the sink term $Q(x)$ such that u and σ can be approximated by linear functions of x at the point of minimal pressure x^* , we have:

$$\begin{aligned} u(x) &= -\frac{\varphi^3}{S^2(1-\varphi)^2} \frac{dp}{dx} \approx -\alpha - \beta x, \\ \text{and } \sigma(x) &= \sqrt{2D_0\varphi^{3/2}} \approx \gamma + \delta x. \end{aligned} \tag{5.5}$$

We are now in precisely the setting where we can follow the parameter rescaling process discussed in Subsection 3.1. This leads to an estimate of the dimensionless parameter η in terms of the proposed benchmark problem:

$$\eta \approx \frac{\delta}{\sqrt{\beta}}.$$

5.2 Numerical simulations

To perform numerical testing in this case, the 1D porous medium equation (5.5) is solved for $p(x)$ using a finite difference method with uniform mesh with $L = 200$. We then use the relation (5.2) and evaluate finite differences to get approximate velocity values u and diffusion coefficient values σ on the grid points. To achieve a smooth representation for the implementation of the SDE solvers, we use the cubic spline to interpolate $u(x)$ and $\sigma(x)$ which can be evaluated at any point in the domain $[0, L]$.

To achieve a range of test cases, we choose parameters (φ, S, D_0) such that $\eta \approx 0.2878 < 0.5$ and $\eta \approx 0.5970 > 0.5$, which we refer to as Case 1 and Case 2 respectively: see the first and second columns in Figure 4 about the linear approximation of $u(x)$ and $\sigma(x)$. We then simulate the mean path of nonlinear SDE (5.1) for the random particle system. If the particles exit the domain $[0, L]$, then we will discard these trajectories. Overall, the mean path of each scheme is averaged over about 895 independent random realizations.

In our two test cases, we simulate the one-dimensional nonlinear SDE (5.1) using the schemes analysed with fine time step size $\delta t = 0.01$ and the coarse time step size $\Delta t = 2$. In these scenarios, all four schemes are still stable regarding the first moment simulation (i.e., mean path), and the numerical results and comparison are summarized in Figure 4. In Case 1 (see the top row of Figure 4) where the effective $\eta \approx 0.2878 < 0.5$, we notice that the RK3 scheme produces least error with coarse time stepping. However, in Case 2, shown in the bottom row, where the effective $\eta \approx 0.5970 > 0.5$, both the SH and EM achieve the best performances, but the error of the SH scheme begins to increase as T becomes larger.

These observations of the nonlinear system agree with the stability analysis of the linear benchmark problem discussed in Section 4, providing strong evidence that the stability analysis of this general linear benchmark example is useful for more complex dynamics.

6 Conclusions

Motivated by the need of practitioners to capture meaningful statistical averages of solutions to SDEs at late times, we derived a family of one-dimensional benchmark problems to evaluate the stability of numerical schemes for SDEs. We used this benchmark to present an analysis of the asymptotic stability of four explicit numerical schemes used for simulating SDEs across a range of convergence orders. We observed that lower-order schemes tend to preserve asymptotic statistical accuracy better than higher-order schemes, a trend which persists in testing of a realistic nonlinear benchmark problem. Natural next steps would be to expand our analysis to include a range of implicit schemes, and to derive similar benchmarks for higher-order and higher-dimensional SDEs.

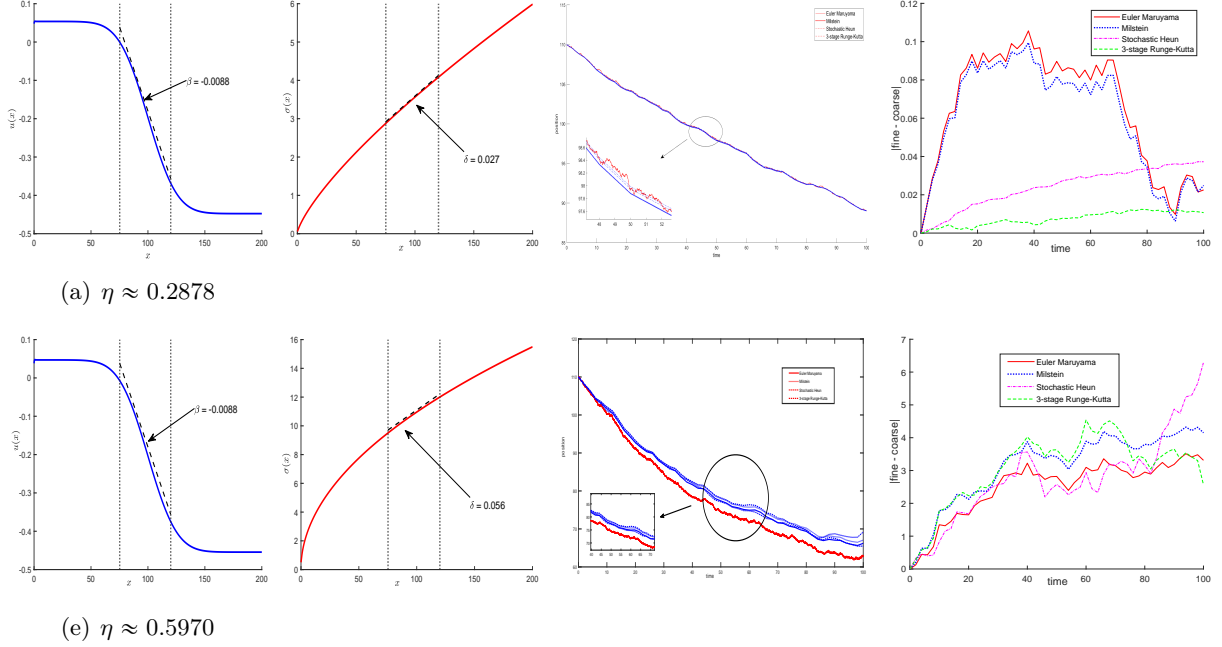


Figure 4: Numerical comparison for stochastic simulation of 1D porous medium (5.1). The velocity and diffusion coefficients and their linear approximations of (5.5) are plotted in the first and second columns. Fine (red) and coarse (blue) mean path and their absolute discrepancies are plotted in the third and fourth columns. Top row is for $\eta < 0.5$ and the bottom row is for $\eta > 0.5$.

Acknowledgements

The authors would like to thank Dr Josephine Evans at University of Warwick for her helpful discussions on the ergodic properties of SDEs during this work.

References

- [1] Eric Cances, Frédéric Legoll, and Gabriel Stoltz. Theoretical and numerical comparison of some sampling methods for molecular dynamics. *ESAIM: Mathematical Modelling and Numerical Analysis*, 41(2):351–389, 2007.
- [2] P.C. Carman. Fluid flow through granular beds. *Chemical Engineering Research and Design*, 75:S32–S48, 1997.
- [3] Douglas Down, Sean P Meyn, and Richard L Tweedie. Exponential and uniform ergodicity of markov processes. *The Annals of Probability*, 23(4):1671–1691, 1995.
- [4] Xiaoying Han, Peter E Kloeden, Xiaoying Han, and Peter E Kloeden. Numerical methods for ordinary and stochastic differential equations. *Random Ordinary Differential Equations and Their Numerical Solution*, pages 101–108, 2017.
- [5] Xiaoying Han and Habib N Najm. Modeling fast diffusion processes in time integration of stiff stochastic differential equations. *Communications on Applied Mathematics and Computation*, 4(4):1457–1493, 2022.
- [6] Xiaoying Han, Mauro Valorani, and Habib N Najm. Explicit time integration of the stiff chemical langevin equations using computational singular perturbation. *The Journal of Chemical Physics*, 150(19), 2019.

- [7] Lars Hörmander. Hypocoelliptic second order differential equations. *Acta Math.*, 119:147–171, 1967.
- [8] Peter Eris Kloeden, Eckhard Platen, and Henri Schurz. *Numerical solution of SDE through computer experiments*. Springer Science & Business Media, 2012.
- [9] Frédéric Legoll, Tony Lelièvre, and Upanshu Sharma. An adaptive parareal algorithm: application to the simulation of molecular dynamics trajectories. *SIAM Journal on Scientific Computing*, 44(1):B146–B176, 2022.
- [10] Gisirô Maruyama. Continuous Markov processes and stochastic equations. *Rend. Circ. Mat. Palermo (2)*, 4:48–90, 1955.
- [11] Jonathan C Mattingly, Andrew M Stuart, and Desmond J Higham. Ergodicity for sdes and approximations: locally lipschitz vector fields and degenerate noise. *Stochastic processes and their applications*, 101(2):185–232, 2002.
- [12] Sean P Meyn and Richard L Tweedie. *Markov chains and stochastic stability*. Springer Science & Business Media, 2012.
- [13] Grigorii Noikhovich Milstein. *Numerical integration of stochastic differential equations*, volume 313. Springer Science & Business Media, 2013.
- [14] G Robert and R Tweedie. Exponential convergence of langevin diffusions and their discrete approximation. *Bernoulli*, 2:341–363, 1996.
- [15] W Rüemelin. Numerical treatment of stochastic differential equations. *SIAM Journal on Numerical Analysis*, 19(3):604–613, 1982.
- [16] Yoshihiro SAITO and Taketomo MITSUI. Discrete approximations for stochastic differential equations. *Trans. Japan SIAM*, 2:1–16, 1992. In Japanese.
- [17] Yoshihiro Saito and Taketomo Mitsui. Stability analysis of numerical schemes for stochastic differential equations. *SIAM Journal on Numerical Analysis*, 33(6):2254–2267, 1996.
- [18] Yoshihiro Saito and Taketomo Mitsui. Mean-square stability of numerical schemes for stochastic differential systems. *Vietnam J. Math*, 30:551–560, 2002.
- [19] Bernhard Tjaden, Samuel J Cooper, Daniel JL Brett, Denis Kramer, and Paul R Shearing. On the origin and application of the bruggeman correlation for analysing transport phenomena in electrochemical systems. *Current Opinion in Chemical Engineering*, 12:44–51, 2016. Nanotechnology / Separation Engineering.
- [20] Angel Tocino and MJ Senosiain. Mean-square stability analysis of numerical schemes for stochastic differential systems. *Journal of Computational and Applied Mathematics*, 236(10):2660–2672, 2012.